

# Effect of Common Chemical Treatments on the Process Kinetics and Mechanical Properties of Flax/Epoxy Composites Manufactured by Resin Infusion

Steven Phillips · Pei-Yu Kuo · Cristian Demaria ·  
Larry Lessard · Mohini Sain · Pascal Hubert

Published online: 8 February 2015  
© Springer Science+Business Media New York 2015

**Abstract** Chemical treatments are widely employed to improve the fiber-matrix adhesion in composites based on eco-friendly fibers such as flax. To better understand the influence of these treatments on processing behavior, this study characterized the surface chemistry and morphology of woven flax fabrics treated by acetone, alkaline, silane and diluted epoxy. Flax/epoxy composites were then manufactured by resin infusion and the flow front and preform thickness evolution was monitored. The alkaline treatment was shown to result in a 50 % increase in equivalent permeability due to an increase in porosity which led to a decrease in flexural properties. The processing results were found to be in good agreement with predictions of a 1-dimensional model. This study suggests that infusion times are not considerably affected by the observed changes in surface energy. However, other implications of the treatments such as an increase in fibrillation can alter the infusion times significantly.

**Keywords** Flax · Surface treatments · Permeability · Consolidation

## Introduction

Flax as well as other bast fibers (which are derived from the stems of certain plant species) has shown good potential in the reinforcement of polymers to produce a class of eco-friendly composite materials [1]. A major drawback of flax fiber-reinforced composites is their limited strength. Part of this limitation arises from the poor adhesion of flax fibers to many common resin systems. Fiber/matrix adhesion is critical in composite materials to distribute load amongst the reinforcement fibers and maximize strength. Of the several methods proposed to improve adhesion, chemical treatment of the fibers is the most commonly used [1, 2]. Although much attention has been given to the influence of these treatments on mechanical properties, little is known about their influence on processing behavior such as permeability and compaction response. These properties are equally as important for cellulose-based fibers as they are for synthetic fibers.

Permeability is a property of porous materials that represents their resistance to fluid flow through them. Consequently, it has a great influence on processing times and flow patterns. Several factors have been shown to influence the permeability of cellulose-based reinforcements, including fiber modification such as chemical treatment [3] as well as reinforcement architecture such as yarn length and diameter [4]. This class of fibers has also been observed to exhibit complex behavior such as swelling and sink effects [5]. These phenomenon are beginning to be understood and a recently proposed model by Masoodi et al. [6] helps to describe these issues. In general, the reported in-plane permeability values for bast fiber reinforcements are much lower for a given fiber volume fraction ( $V_f$ ) when compared with conventional fibers [7, 8]. There is evidence that suggests that the use of chemical

---

S. Phillips (✉) · C. Demaria · L. Lessard · P. Hubert  
Department of Mechanical Engineering, McGill University,  
817 Sherbrooke Street West, Montreal H3A 0C3, Canada  
e-mail: steven.phillips@mail.mcgill.ca

P. Hubert  
e-mail: pascal.hubert@mcgill.ca

P.-Y. Kuo · M. Sain  
Faculty of Forestry, University of Toronto, 33 Willcocks Street,  
Toronto M5S 3B3, Canada

treatments can change the measured permeability of cellulose-based fabrics due to physical and chemical changes [3]. This in turn alters the flow kinetics of a class of composite manufacturing processes known as liquid composite moulding (LCM) processes. This flow behavior has been shown to be dual-scale in nature and comprise of both macro-flow in the inter-tow region as well as micro-flow in the intra-tow region [9, 10]. The micro-flow largely depends on the capillary pressure (especially in low pressure processes such as resin infusion) whereas the macro-flow is affected to a much lesser extent [11]. Due to changes in surface energy, the use of chemical treatments will inherently result in changes in capillary pressure and consequently injection time. This has been observed for the case of glass/polyester composites [12]. For the case of bast fiber-composites, Rodriguez et al. [3] studied the effect of alkaline treatment on the mechanical properties and process kinetics of jute/vinyl ester composites. They determined that the alkali treatment collapsed the hollow center of jute fibers (known as the lumen) and consequently limited the micro-flow and increased the overall process time. Furthermore, it was found that the permeability decreased for a constant fiber  $V_f$  due to an increase in fiber roughening.

Along with permeability, the compaction behavior (i.e. the response of the fiber bed to consolidation pressure) plays a crucial role in LCM processes due to its direct influence on permeability. Many variables have been reported to play a role in the compaction behavior of cellulose-based fabrics including the fiber mechanical properties, fabric architecture, loading rate and lubricating effects [13]. For the case of cellulose-based fabrics, it has generally been observed that higher mould clamping forces are required to attain similar fiber  $V_f$  to that of conventional reinforcements [14–16]. In addition, changes in the fiber structure have been observed such as the collapse of the lumen [15].

Taking all of the above into account, it is clear that the above issues must be addressed in order for these eco-friendly reinforcements to become more desirable in terms of processing. Furthering the understanding of the implications of chemical treatments is one step in potentially improving the process-ability of this class of fibers. To date, few studies have considered the implications of these treatments in the resin infusion process. Resin infusion is an LCM process that makes use of a one-sided tool and flexible vacuum bag. The flexible nature of the vacuum bag results in the coupling of the permeability and compaction behavior of the fiber bed which makes the process particularly sensitive to changes in fiber and fabric properties. A schematic of the main steps involved in this process is presented in Fig. 1.

The process begins with the preform placement onto the tool surface along with a layer of peel ply (a permeable

release film). This is sometimes accompanied by a distribution media which is an optional layer that speeds up the process when the permeability of the preform is low. Spiral tubing is then often incorporated in the bagging arrangement to act as the resin inlet and vent. The layup is then covered with a vacuum bag and vacuum is drawn on the dry preform, initiating the ‘pre-filling’ stage. The inlet tube is then opened which initiates the flow of resin and the ‘filling’ stage. Following saturation of the preform, the inlet tubing is typically clamped and the ‘post-filling’ stage commences. After the system reaches equilibrium, the curing of the resin is carried out after which the part is removed from the tool.

The current study aims to understand the implications of common chemical treatments on the process kinetics and mechanical properties of woven flax/epoxy manufactured by resin infusion. This paper begins with a description of the fiber treatment methods as well as a characterization of the treated fibers by fourier transform infrared spectroscopy (FTIR), scanning electron microscopy (SEM) and advancing contact angle analysis. This is followed by a description of experiments where the kinetics of the resin infusion process was monitored during the manufacturing of flax/epoxy laminates. The evolution in flow front is compared to predictions of a 1-dimensional resin infusion process model for which the saturated permeability and wet unloading behavior of the fabric is quantified. Finally, a mechanical characterization is presented on the cured laminates and some insight is given into the implications of the studied chemical treatments on the processing of flax fiber reinforcements.

## Materials

Woven flax fabrics ( $2 \times 2$  twill weave) with an areal weight of  $550 \text{ g/m}^2$  were kindly supplied by Libeco-Lagae® (Meulebeke, Belgium). An epoxy resin system with low viscosity and long pot life was selected for the sample manufacturing, namely Huntsman Araldite LY1564 and Aradur 3486 (Sacramento, California, USA). For the saturated permeability and wet unloading experiments, Dow Corning® Fluid 200 silicone oil (Midland, Michigan, USA) was employed. The viscosity of both fluids was determined in the temperature range of interest ( $24\text{--}27^\circ \text{C}$ ) with a TA AR2000 rheometer equipped with a  $2^\circ$  cone and 40 mm diameter plate geometry. A flow test employing a frequency sweep from 10 to 500 Hz was carried out and the viscosity was taken to be that measured at 500 Hz. The viscosity ( $\mu$ ) in Pa·s over the given temperature range was then fit using an Arrhenius model of the form:

$$\mu = \mu_0 e^{-\frac{E}{RT}} \quad (1)$$

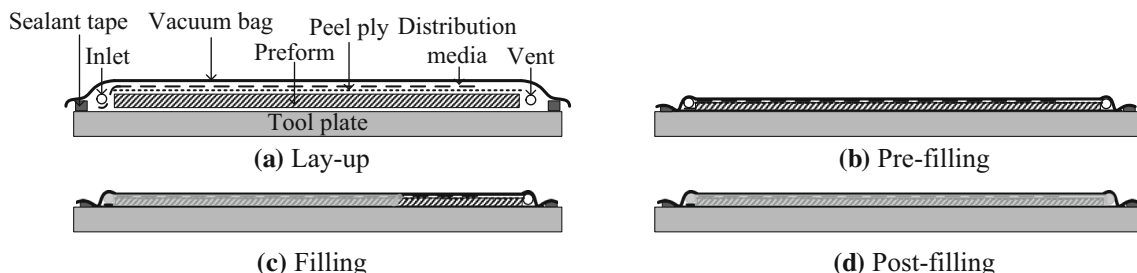


**Fig. 1** Steps involved in the resin infusion process; **a** lay-up, **b** pre-filling, **c** filling and **d** post-filling

where  $T$  is the absolute temperature (K),  $\mu_0$  is a constant (Pa s),  $R$  is the universal gas constant (8.314 J/K/mol) and  $E$  is the activation energy (J/mol). For the epoxy resin, the constant and activation energy were determined to be  $7.268 \times 10^{-10}$  Pa·s and  $-5.001 \times 10^4$  J/mol respectively. For the silicone oil, they were determined to be  $5.013 \times 10^{-4}$  Pa·s and  $-1.292 \times 10^4$  J/mol respectively.

**Fabric Characterization**

Following the material selection, the fabrics were subjected to chemical treatments and characterized by FTIR, SEM and advancing contact angle analysis. The results from these tests are described in the following subsections.

**Chemical Treatment**

Four chemical treatments were selected based on the work of Van de Weyenberg et al. [2] and are summarized in Table 1. The first solution was acetone which was intended to remove potential impurities from the as supplied fabrics. The second was a 4 % NaOH aqueous solution (alkaline treatment). This treatment was followed by washing with distilled water until a balanced pH level was measured by litmus paper. The third treatment was a 1 % silane of type gamma-glycidoxypropyltrimethoxysilane in a solution of 60 % ethanol and 40 % distilled water (pH between 3.5 and 4). The final treatment was a 3 % diluted epoxy in acetone. The epoxy monomer and hardener were first mixed in acetone into which the fabrics were added. Following all treatments, the fabrics were dried for 12 h at

80 °C in a convection oven. An exception was the diluted epoxy treatment which was dried at ambient conditions.

**Fourier Transform Infrared Spectroscopy**

To understand the effect of the treatments on the fiber functional groups, FTIR was carried out on a Bruker ATR instrument. A spectrum from 4,000 to 400  $\text{cm}^{-1}$  was selected with a resolution of 4  $\text{cm}^{-1}$ . The signals were analyzed in OPUS software and the results are shown in Fig. 2. It was found that the untreated flax fibers showed characteristic bands for cellulose-based fibers including the hydrogen bonded OH stretching at 3,600–3,080  $\text{cm}^{-1}$ , the CH stretching at 2,970–2,860  $\text{cm}^{-1}$ , the CH<sub>2</sub> bending at 1,450–1,430/1,360  $\text{cm}^{-1}$ , the C–O stretching at 1,058 and 1,035  $\text{cm}^{-1}$  and the CH bending at 900  $\text{cm}^{-1}$  (which indicates the amorphous structure). The spectrum of acetone treated fiber does not show any significant difference. However, the absorption peak of OH groups for the alkali-treated fibers shifted to a lower wave number near 3,280  $\text{cm}^{-1}$ . This implies that the degree of hydrogen bonding between OH groups increased. On the contrary,

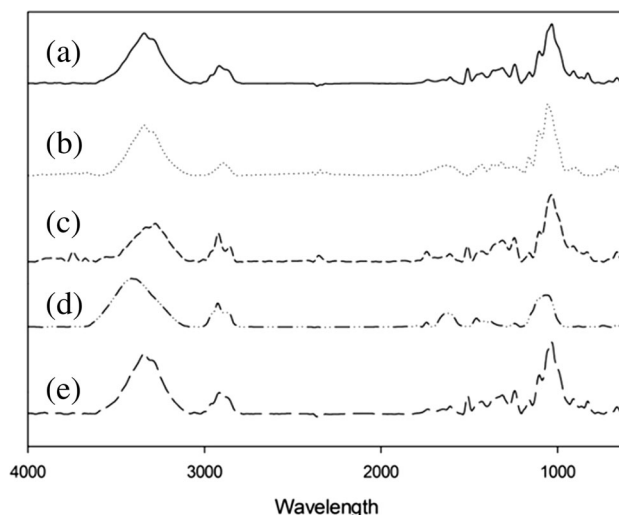


**Fig. 2** Spectrography from FTIR on treated flax fibers: *a* untreated, *b* acetone, *c* alkaline, *d* silane and *e* diluted epoxy

**Table 1** Chemical treatment parameters applied to flax yarns

Treatment	Concentration (%)	Time (h)	Temperature (°C)
Acetone	100	2	23
Alkaline	4	2	23
Silane	1	2	23
Diluted epoxy	3	2	23

the absorption peak for the silane-treated fibers was shifted to a higher wave number to the position of free OH groups. Another characteristic absorption peak of silane was around  $1,000\text{--}1,100\text{ cm}^{-1}$ . This could be attributed to the presence of the asymmetric stretching of Si–O–Si and/or Si–O–C bonds.

### Scanning Electron Microscopy

SEM was carried out to observe the effect of the treatments on the surface morphology. Small sections of the fabrics were gold-coated and images were captured in an SEM (Fig. 3). The SEM images provided some insight into the nature of the treatment on the fiber surfaces. Most distinct was the diluted epoxy treatment which displayed clear epoxy droplets in a non-uniform manner. The untreated, acetone, alkaline and silane treatments did not reveal any significant differences. Alkaline treatments have been observed by other authors to roughen the surface of bast fibers [17]. However, this outcome was not obvious in the current study likely due to the relatively low concentration of the NaOH solution. The SEM imaging suggested that the uniformity of the treatments (especially in the case of the diluted epoxy) on the surface and inside of the yarns was an important factor.

### Contact Angle Measurement

To understand the change in fiber surface energy, advancing contact angle analysis was carried out on a Kruss K100

dynamic tensiometer using the Wilhelmy plate method. Technical flax fibers composing of five to ten elementary fibers were selected from the treated flax yarns. A displacement rate of  $1.5\text{ mm/min}$  was applied during the advancing contact angle measurement. The receding angle was not studied since, during this stage, the fiber was already wet by the test fluid and the contact angle approached zero. The test fluids that were selected were pure water, diodomethane and ethylene glycol. The surface energy component of these fluids were obtained from Volpe et al. [18]. Owens–Wendt theory was applied to deduce the polar and dispersive components of the total surface energy as given by [19]:

$$\gamma_L \frac{(\cos \theta + 1)}{2\sqrt{\gamma_L^D}} = \frac{\sqrt{\gamma_S^P}\sqrt{\gamma_L^P}}{\sqrt{\gamma_L^D}} + \sqrt{\gamma_S^D} \quad (2)$$

where  $\gamma$  is the surface energy and  $\theta$  is the contact angle. Subscripts S and L represent the solid and liquid respectively. Superscripts P and D represent the polar and dispersive components respectively. The contact angle was determined from the Wilhelmy equation given by [20]:

$$\cos \theta = \frac{F}{\gamma \times l} \quad (3)$$

where  $F$  is the force measured by the tensiometer micro-balance,  $\gamma$  is the surface tension of the test fluid and  $l$  is the perimeter of the fiber. To account for buoyancy forces, the plot of contact angle versus position was extrapolated to zero. To account for the weight of the sample and fixture, the balance was zeroed prior to testing.

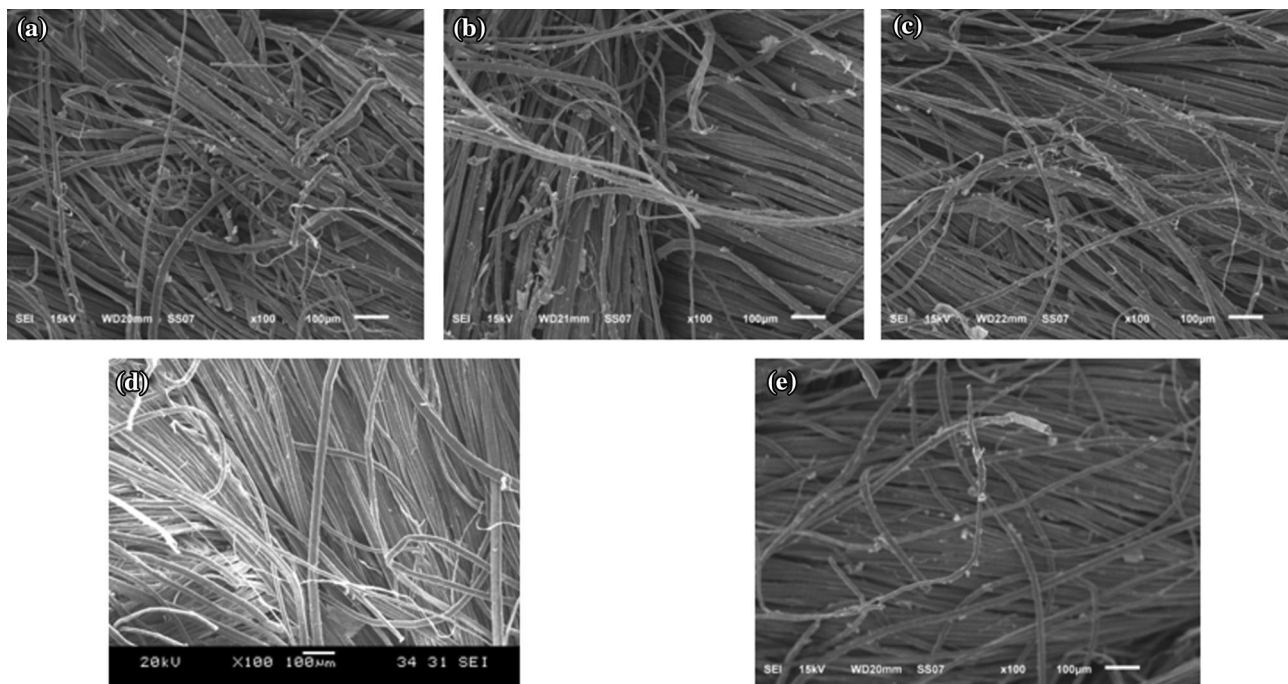


**Fig. 3** SEM images of treated flax fibers: **a** untreated, **b** acetone, **c** alkaline, **d** silane and **e** diluted epoxy

The perimeter of the fiber was measured using a fully wetting fluid, n-hexane, in order to approach a contact angle of zero. The diameter was then deduced from Eq. 3. To verify this method, ten fiber cross-sections were also measured by optical microscopy. The two methods were found to be within 15 % of each other which was deemed acceptable.

As can be seen from Eq. 2, a linear plot can be made whereby the polar and dispersive components of the surface energies can be determined from the slope and y-intercept. The line coefficient,  $R^2$ , of this plot varied between 0.88 and 0.99. The surface energies determined from the slope and y-intercept are given in Table 2 where  $\gamma_p$ ,  $\gamma_d$  and  $\gamma_t$  represent the polar, dispersive and total surface free energies respectively.

The results indicate that, for the majority of the selected treatment parameters, there was not a significant change in fiber surface chemistry. Exceptions were the silane and diluted epoxy treatment which showed a large reduction in the polar component. The alkaline treatment did not show a large change likely due to the relatively low concentration of the NaOH solution [17]. The as supplied fabric agreed well with surface energy values reported by Cantero et al. [21].

### Composite Processing

The processing portion of this work consisted of monitoring the flow front evolution and thickness change in a

**Table 2** Surface energies for treated flax fibers ( $\pm$ SD)

Treatment	$\gamma_p$ (mJ/m <sup>2</sup> )	$\gamma_d$ (mJ/m <sup>2</sup> )	$\gamma_t$ (mJ/m <sup>2</sup> )
Untreated	25.6 $\pm$ 2.6	16.5 $\pm$ 1.0	42.1 $\pm$ 3.6
Acetone	22 $\pm$ 3.0	18.4 $\pm$ 0.9	40.5 $\pm$ 3.9
Alkaline	22.9 $\pm$ 3.4	16.3 $\pm$ 0.7	39.2 $\pm$ 4.1
Silane	11.4 $\pm$ 3.9	19.5 $\pm$ 2.0	30.8 $\pm$ 5.9
Diluted epoxy	3.5 $\pm$ 0.8	22.2 $\pm$ 0.9	25.7 $\pm$ 1.7

series of infusion experiments using the treated fabrics from Sect. 3. The experimental setup, procedure and process data are discussed below.

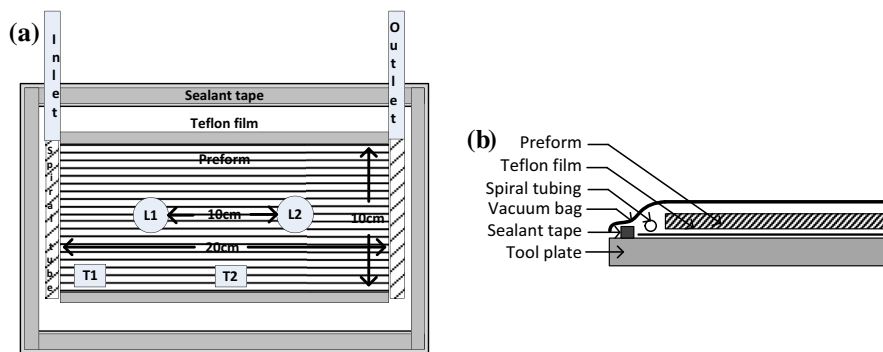
### Setup

An instrumented tool plate suitable for resin infusion was constructed for the infusion experiments (Fig. 4). The setup was attached to a hot plate to accelerate curing of the resin. A pressure transducer (Wika Eco-Tronic) was connected to a resin trap at the outlet to monitor the vacuum pressure. Laser thickness sensors (Banner LG5A65NIQ) that employed optical triangulation, were installed at two positions as denoted by  $L_1$  and  $L_2$  in Fig. 4. The flow front was tracked visually at 2 cm intervals. To prevent race tracking, the sides of the preforms were lined with sealant tape.

### Procedure

Each test began with a leak check consisting of detaching the vacuum line and monitoring the pressure in the resin trap. An increase of approximately 0.05 kPa over 10 min was observed which was deemed acceptable. The pre-filling stage, which consisted of the preform compaction in a dry state, was then recorded. A 1 h debulk was performed after to encourage moisture removal. The resin was mixed by hand for 5 min and degassed for 30 min during the debulk stage. The infusion then took place during which the flow front was tracked visually by recording the time at 2 cm intervals. During this phase, the thickness evolution was also monitored by the laser thickness transducers. The inlet tube was then clamped at the moment the resin reached the end of the preform. The system was finally held for 1 h at ambient conditions to monitor the post-fill stage before starting the cure cycle. A cure temperature and time of 50 °C and 12 h respectively were selected. A minimum of three laminates were manufactured for each chemical treatment.

**Fig. 4** Schematic of infusion setup; **a** top view and **b** side view



Preliminary experiments revealed that the resin tended to degas under very low vent pressures. To alleviate this issue, the resin was degassed at about 0.5 kPa lower pressure than that which was set at the vent during the filling stage using a vacuum regulator. Furthermore, two additional post-fill pressures (25 and 50 kPa) were included in the design of experiments to produce composites of varying void content so that the effect of voids on flexural and Charpy impact properties could be studied.

### Process Kinetics

The three stages of the resin infusion process described in Fig. 1 were recorded on the instrumented tool plate during the laminate manufacturing. A discussion of the data recorded from these stages as well as a comparison of the equivalent permeability values computed during the filling stage is presented below.

#### Pre-Filling

During the pre-filling stage, the fibrous preform was compacted in a dry state. Average dry compaction curves are shown in Fig. 5. Since the behavior was measured following a leak test, it represented the behavior of the fiber bed after one compaction cycle. The fiber  $V_f$  was calculated from:

$$V_f = \frac{\eta \cdot \alpha}{\rho \cdot h} \quad (4)$$

where  $\eta$  is the number of layers,  $\alpha$  is the areal weight of the fabric,  $\rho$  is the density of the fiber and  $h$  is the thickness of the preform (as measured by the laser sensors). A fiber density of 1.5 g/cm<sup>3</sup> [1] was assumed. A fabric areal weight of 543 g/m<sup>2</sup> was measured on five 20 × 35 cm<sup>2</sup> untreated fabric sections after being dried at 110 °C for 1 h in a convection oven. The fiber density and fabric areal

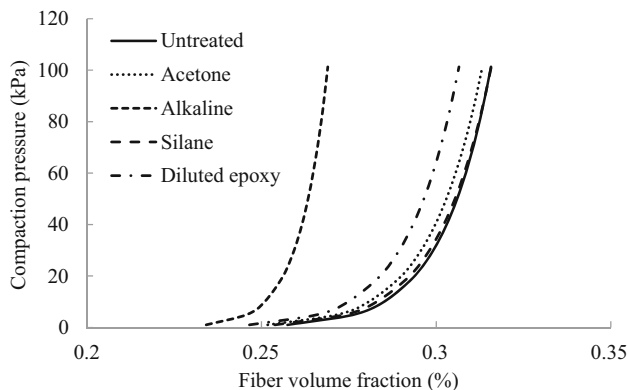


**Fig. 5** Average compaction pressure versus fiber volume fraction for 3 layers of dry flax fabric treated by common chemical treatments

weight were assumed to be constant for the different treatments. The latter was determined for the treated fabrics from an average measurement of four 10 × 15 cm<sup>2</sup> sections after 48 h exposure in a desiccant chamber and was found to vary negligibly (<2 %). Since the treated fabrics did not change in areal weight, the constant fiber density assumption was deemed acceptable. It should be noted that some studies have shown a change in “apparent” density due to the alkaline treatment of cellulose-based fibers [22, 23]. However, the apparent density does not account for the porosity that is created due to the removal of pectin, lignin and hemicelluloses from the fiber and would thus be misleading in the computation of fiber  $V_f$ .

To quantify the measured compaction behavior, the data was fit using a power-law as suggested by Robitaille et al. [13] (Table 3). The power-law took the form:

$$V_f = A\sigma^B \quad (5)$$

where  $A$  (kPa<sup>-B</sup>) and  $B$  are fitting constants and  $\sigma$  is the applied stress (in kPa). The pressure range from 10 to 100 kPa was used in fitting the model, as incorporation of very low pressures (<10 kPa) resulted in an inferior fit and was deemed unnecessary since such low compaction pressures only occurred in the immediate vicinity of the inlet during the process. The  $R^2$  value was at least 0.95 for all the experimental data which was deemed acceptable for the purposes of this study. It can be seen from Fig. 5 and Table 3, that there was not generally a large difference in dry compaction behavior. However, the alkaline treatment showed much lower fiber  $V_f$  for a given pressure. This was likely due to the apparent swelling which alkaline treatments induce in cellulose fibers as a result of increased fibrillation due to the removal of lignin, pectin and hemicellulose [1]. This would have caused more fiber–fiber contact points and thus would have increased the required load to attain a given fiber  $V_f$ . This apparent swelling effect is commonly minimized by tensioning the fabrics during treatment [24]. Therefore, for the purpose of composite processing, the fabric boundary condition during the alkaline treatment plays a key role. Similar to the alkaline treated fabrics, those treated by diluted epoxy showed the

**Table 3** Average power-law constants for dry compaction behavior of flax fabric subjected to chemical treatments

	A (kPa <sup>-B</sup> )	B	$V_{fmax}$
Untreated	0.257	0.0442	0.316
Acetone	0.251	0.0474	0.313
Alkaline	0.234	0.0300	0.269
Silane	0.253	0.0474	0.316
Diluted epoxy	0.246	0.471	0.306

same trend to a much lesser extent. This was likely due to stiffening of the fabric as a result of the epoxy. This stiffening probably also caused a reduction in yarn ‘nesting’ (i.e. the packing of yarns from different layers) which can assist in achieving higher fiber  $V_f$  for multi-layered preforms [13].

*Filling and Post-Filling Stage*

The evolution of thickness for the untreated fabrics during the filling and post filling stages is shown in Fig. 6a at the positions of laser sensors 1 and 2. The behavior was typical of that observed during the resin infusion process. The fabrics first underwent wet unloading as the resin advanced and gradually carried more of the applied load. This was followed by wet compaction as a result the inlet clamping and subsequent removal of excess resin. As shown in Fig. 6b, the final fiber  $V_f$  tended to decrease with increasing vent pressure during the post-fill stage (due to the removal of less resin). Similar to the pre-filling stage, the difference in behavior for most of the treatments was not pronounced. However, the alkaline treatment again clearly exhibited much lower fiber  $V_f$  throughout the filling and post-filling stages.

*Equivalent Permeability Comparison*

For comparative purposes, the equivalent permeability values during the filling stage were computed (Fig. 7). The equivalent resin infusion permeability neglects the thickness change during the process and assumes a constant porosity [25]. Assuming full saturation behind the flow front, the equivalent permeability can be derived from Darcy’s law as:

$$K = \frac{m \cdot \phi \cdot \mu}{2 \cdot (p_{applied} + p_c)} \tag{6}$$

where  $m$  is the slope of flow front position squared versus time,  $\phi$  is the porosity,  $\mu$  is the viscosity,  $p_{applied}$  is the applied pressure gradient and  $p_c$  is the capillary pressure. The last of these parameters is often neglected due its small magnitude in comparison to the applied pressure. However, during the resin infusion process its magnitude can be comparable due to the relatively low pressure gradient involved. In the case of bast fibers, the capillary pressure can exceed 30 % of the applied pressure depending on the resin type and porosity range [26]. For orthotropic fiber textiles, capillary pressure can be calculated from a modified Young–Laplace equation given by [27]:

**Fig. 6** Filling and post-filling stage processing kinetics **a** thickness evolution for untreated flax fabric at 5 kPa vent pressure **b** fiber volume fraction before and after post-fill stage for treated flax fabrics (average of both laser sensors)

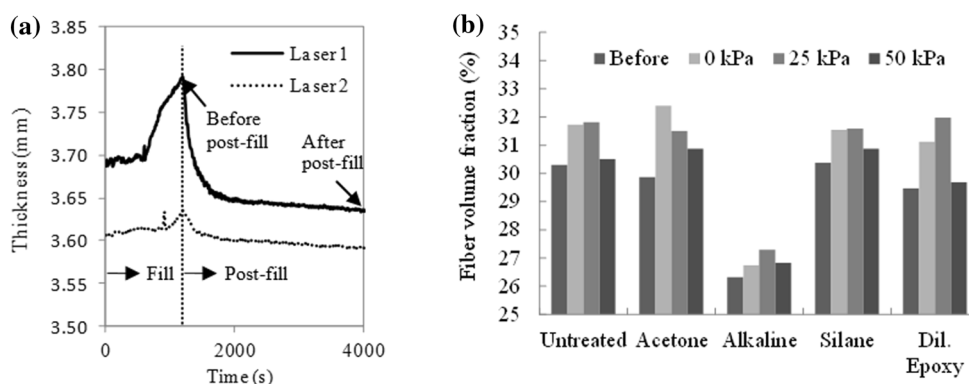
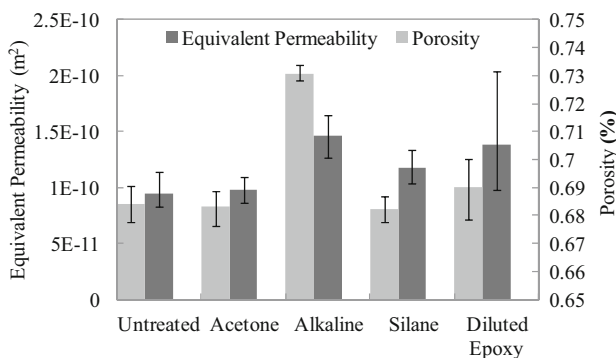


**Fig. 7** Equivalent permeability and porosity during resin infusion process for flax fabrics treated by common chemical treatments (error bars represent maximum and minimum values)



$$p_c = \frac{F}{D_f} \cdot \frac{(1 - \varphi)}{\varphi} \cdot \gamma \cdot \cos \theta \quad (7)$$

where  $D_f$  is the diameter of a single fiber,  $\varphi$  is the porosity,  $\gamma$  is the surface tension of the resin,  $\cos \theta$  is the contact angle and  $F$  is a form fitting factor which depends on the textile architecture. In the current study, the contact angle with the epoxy resin was determined from the Owens–Wendt equation (Eq. 2) using literature surface energy values for a similar epoxy reported by Comyn [28] ( $\gamma_d = 41.2$ ;  $\gamma_p = 5.0$  mJ/m<sup>2</sup>). The form fitting factor was assumed to be the same as a plain weave carbon fabric (3.84 [29]) and the fiber diameter was taken to be 17.8  $\mu\text{m}$  [30]. Based on these inputs, the capillary pressure was estimated to range from 2 kPa for the diluted epoxy treated fabrics to 4 kPa for the untreated fabrics. Upon examination of Eq. 7, these low values of capillary pressure were mainly a result of the high porosity values.

The results suggest that, in general, the use of chemical treatments did not result in significant changes in the equivalent permeability for resin infusion. An exception was again the alkaline treatment which showed a distinct increase in equivalent permeability mostly due to an increase in porosity. In the case of the silane and diluted epoxy treatments, analysis-of-variance (ANOVA) revealed that the permeability differences were not statistically significantly different from the untreated fabrics based on the Scheffe criterion. A large degree of scatter for the diluted epoxy treatment was likely a result of the non-uniformity of the applied treatment as was seen in the SEM images. Therefore, similar to the alkaline treatment, the method of treatment must be chosen appropriately in order to obtain the desired result.

## Process Modelling

To get a better understanding of the processing results, the flow front evolutions from the previous section were compared with predictions from a 1-dimensional resin infusion process model. The model development and predictions are presented below. Additionally, the quantification of two key model parameters are presented; the wet unloading of the fiber bed and permeability over the relevant range of fiber  $V_f$ . It should be noted that the characterization was carried out only for the untreated fabrics and the behavior of the treated fabrics was assumed to be the same. Although this was likely not a valid assumption, the purpose of the modelling was to isolate to effect of the observed changes in surface energy as well as to see how well a simple 1D process model predicted the evolution in flow front for the untreated fabric.

## Model Development

The 1D resin infusion model that was selected for comparison was that developed by Hammami et al. [31] where the governing equation was given by:

$$\frac{\partial}{\partial x} \left( \frac{Kh}{\mu} \frac{\partial p}{\partial x} \right) = 0 \quad (8)$$

where  $K$  is the permeability,  $h$  is the preform thickness,  $\mu$  is the viscosity and  $p$  is the pressure. In the current study, the model differed in terms of the boundary equations. Instead of neglecting capillary pressure at the flow front, the following boundary conditions were imposed:

- at  $x = 0$ ;  $p = p_{\text{atm}}$
- at  $x = x_f$  (flow front);  $p = p_v - p_c$

where  $p_{\text{atm}}$ ,  $p_v$  and  $p_c$  are the atmospheric, vacuum and capillary pressure respectively. The last of these pressures is given by Eq. 8 and depends on the preform porosity. However, since the porosity was constant at the flow front, the capillary pressure was also constant at the flow front. Equation 8 was solved using a finite difference scheme over the interval from  $x = 0$  to  $x = x_f$ . The number of nodes was set to ten. To determine the velocity at the flow front, Darcy's law was solved at the last two nodes of the discretized pressure field to determine the interstitial velocity (i.e. the velocity experienced by the fluid in the pores). The new flow front position was then determined using a time step of 1 s and the velocity at the flow front. Two key material parameters for the model were the wet unloading and the permeability of the fabric. The characterization of these parameters is described in the following subsections.

## Permeability

The permeability measurement setup was based on the work of Croteau-Labouly [32]. It made use of changes in porosity experienced by the fiber bed during the resin infusion process to compute saturated permeability values over a limited range of fiber  $V_f$ . It should be noted that during the resin infusion filling stage, the fiber bed is not strictly saturated. However, saturated permeability was selected for the model since, for the infusion times in this study, fiber swelling due to fluid absorption has been previously reported to be small (<2 %) for bast fibers exposed to non-polar fluids [5]. In addition, visual inspection during the infusions did not reveal any remarkable unsaturated regime.

A schematic of the tool plate design for the test setup is shown in Fig. 8. Five evenly spaced pressure transducers (Omega<sup>®</sup> PX26) and two laser thickness transducers (same as described in Sect. 4.1) were employed. The inlet and



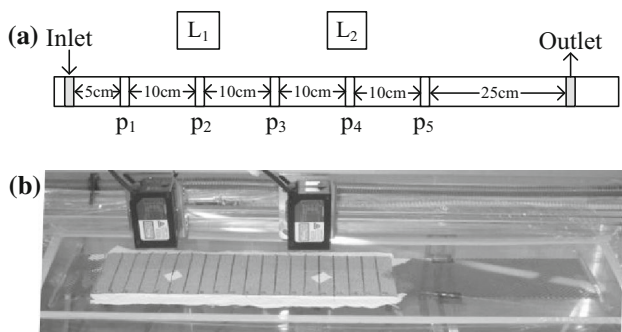


**Fig. 8** Tool plate design for in-plane permeability measurement (where L = laser thickness sensors and p = pressure sensors); **a** side view schematic and **b** actual setup

outlet of this setup were tube fittings that facilitated direct connection with ¼ in. tubing. The bagging arrangement was the same as that shown in Fig. 4 without the release film. A silicone sealer (DAP® AlexPlus®) was used on the sides of the preforms to avoid race tracking. One layer of distribution media was used at the inlet (before p<sub>1</sub>) and outlet (after p<sub>5</sub>) so that the vacuum bag did not seal directly on the tool plate. To measure the flow rate in this apparatus, the resin container was placed on a scale (Ohaus® Scout® Pro SP2001) and the mass change was recorded by a LabView® program.

The experimental procedure was similar to that described in Sect. 4.2. Since silicone oil was used as the test fluid, no degassing was carried out. During the saturated regime, the infusion was carried out until the flow rate and pressure gradient stabilized. The volumetric flow rate was determined from the mass flow rate using the density of the silicone oil (0.971 g/cm<sup>3</sup>). The pressure gradient during the saturated regime was recorded for calculation of the permeability values. By simultaneously characterizing the wet unloading behavior (described in Sect. 5.3), the thickness profile along the length of the preform could also be determined during the saturated regime (Fig. 9).

It is apparent in Fig. 9 that the pressure at the beginning of the preform was above atmospheric pressure and at the end of the preform was below the vacuum level (about 4.75 kPa). This is a result of the resistance to flow due to the distribution media. Although the permeability of this layer was relatively high, the vacuum bag tended to contact the tool plate directly through the distribution media and reduce the permeability. To avoid this, several layers of distribution media can be stacked [32]. However, since the pressure was measured at the beginning and the end of the preform, this was not necessary in the current study.

The compaction pressure at the pressure sensor locations was calculated from Terzaghi’s law which describes the load sharing nature of the fiber bed and resin, given by [33]:

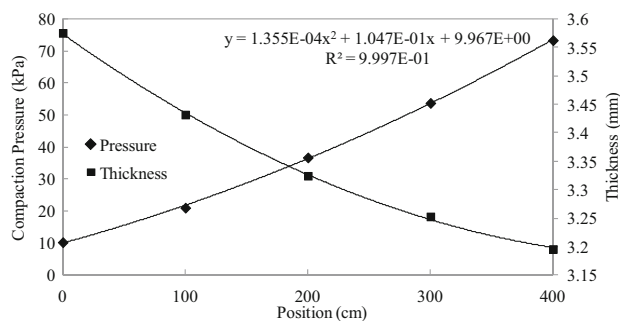


**Fig. 9** Representative spatial variation of pressure and thickness during saturated regime of infusion permeability measurement of woven flax fabric

$$\sigma = \sigma_f + \sigma_r \tag{9}$$

where  $\sigma$ ,  $\sigma_f$  and  $\sigma_r$  are the applied, fiber bed and resin pressures respectively. The pressure data in Fig. 9 followed a 2nd order polynomial. Based on the derivative of this function, the saturated permeability was then computed along the length by rearranging Darcy’s law such that:

$$K = \frac{v\mu\phi}{\frac{\partial p}{\partial x}} \tag{10}$$

where  $v$  is the interstitial velocity,  $\mu$  is the test fluid viscosity,  $\phi$  is the fabric porosity and is the derivative computed from Fig. 9. Following the above calculations, the saturated permeability-fiber  $V_f$  relationship was determined (Fig. 10). It can be seen in Fig. 10 that for the limited range of porosities witnessed in the resin infusion process, a power-law model provides a good fit to the experimental data.

Using the above procedure, a total of four samples were tested and an average was obtained for the permeability-fiber  $V_f$  relationship over the range of observed porosities. The average power-law constants were found to be  $2.39 \times 10^{-15} \text{ m}^2$  and  $-9.12$ .

### Compaction

The other critical property for the model was the transverse deformation behavior of the fiber bed during the filling stage. During this stage, the preform experiences unloading in a wet state as the resin gradually carries more of the applied load as dictated by Eq. 9. It should be noted that there is also a brief period of wet compaction due to the lubrication effect when it is initially wet by the resin [34]. However, this stage is brief and for simplicity it was neglected in the process model. The wet unloading characterization was carried out in situ during the permeability measurements described in Sect. 5.2 through use of the laser thickness transducers. This test method was well

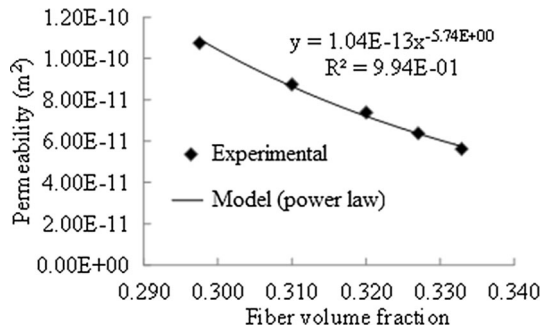


**Fig. 10** Representative permeability versus fiber volume fraction relationship for saturated permeability measurement

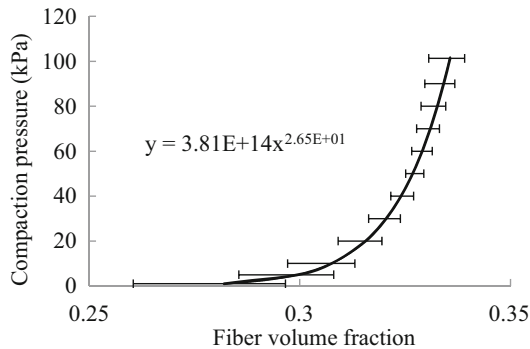


**Fig. 11** Average wet unloading behavior of 3 layers of untreated flax fabric (error bars represent max and min values)

suiting due to the same range of pressures and strain rates involved as the resin infusion process. Only the data recorded by the first thickness transducer ( $L_1$  in Fig. 8) was used to determine the empirical model since a larger range of fiber  $V_f$  was inherently experienced by this sensor. Since the fluid pressure was known at the position of  $L_1$ , the load carried by the fiber bed was determined by Eq. 9. The fiber  $V_f$  was then calculated from Eq. 4 to produce Fig. 11. The power law constants defined in Eq. 5 were  $A = 0.282 \text{ kPa}^{-0.0377}$  and  $B = 0.0377$ .

### Model Validation

With quantification of the permeability and wet unloading behavior, the predictions from the process model were compared to the results from the infusion experiments conducted in Sect. 4.3.3. As in Sect. 4.3.3, the contact angle between the fiber and resin was determined from Eq. 7. The viscosity in the model was taken to be the average for all experiments. As can be seen in Fig. 12, the model predictions were reasonably close to the observed flow front evolutions for the untreated fabric. It should be noted that due to the high variability of the material, there was a relatively large range of error for the time to reach a

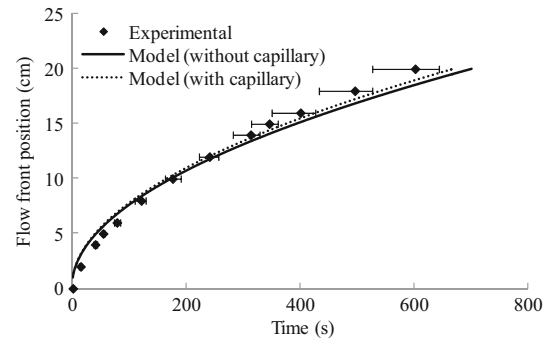


**Fig. 12** Comparison of model predictions and experimental flow front evolutions for epoxy through untreated flax fabric (error bars represent max and min values)

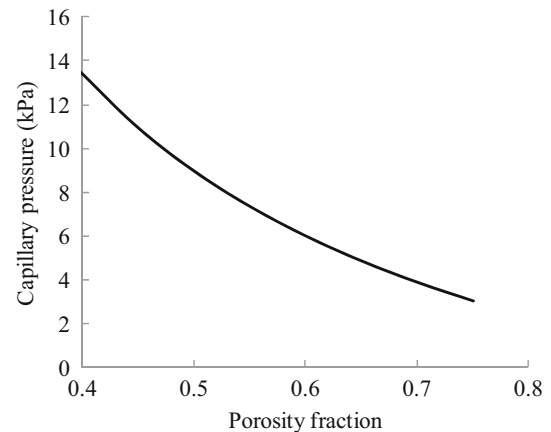


**Fig. 13** Capillary pressure versus fabric porosity as calculated from Eq. 4

given flow front position. Comparing the average flow front position to the model prediction, it can be seen that early on in the process, the model tended to over predict the flow front position while later on it tended to under predict this position. This suggests that fiber swelling was not significant for the studied scenario since swelling would have resulted in lower permeability later on in the process and consequently a slower flow front evolution. In any case, the effect of capillary pressure predicted by the model was slight, due to the low ranges of porosity for the studied fabric system in the given porosity range. However, capillary pressure could have been non-negligible (exceeding 10 kPa) if lower ranges of porosity had been achieved (Fig. 13). Based on the measured surface free energy values reported in Sect. 3.4, the effect of fiber surface free energy on the flow front evolution was also investigated. However, due to the low range of porosity for the fabric system investigated there was a negligible difference in flow kinetics for the various treatments. During the analysis, the wet unloading behavior of the treated fabrics was

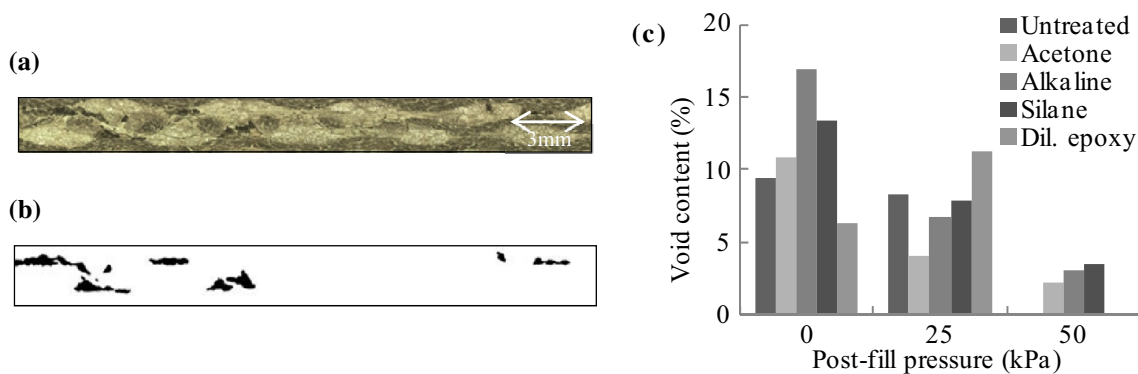


**Fig. 14** Void analysis results; **a** selected cross-section, **b** cross-section after thresholding and **c** void content versus post-fill pressure

assumed to be the same as the untreated fabrics. Therefore, the predictions do not take into account other changes that result from the chemical treatments such as changes in fiber surface morphology or fabric porosity. The results from the infusion experiments in Sect. 4.3 indicate that these factors are significant for some treatments (e.g. alkaline). In LCM processes such as resin transfer moulding (RTM), these changes may not be as significant since the cavity thickness is constant and the mould clamping force can be adjusted. However, due to the unique coupled flow and compaction behavior of the resin infusion process, some treatments such as alkaline can result in significant changes in the equivalent permeability. Therefore, simply looking at the capillary pressure to understand changes in process kinetics does not provide the complete story. To accurately model the effect of these changes, the differences in fiber and fabric morphology must be taken into account.

### Mechanical Characterization

As a last step after curing the composites manufactured in Sect. 4, a mechanical characterization was carried out. The following tests were carried out and the results are presented below; void analysis, flexural and Charpy impact.

#### Void Analysis

Void analysis was carried out by optical microscopy and image analysis on a 5 cm long polished cross section from the center of each laminate. Due to the limited contrast between the voids and the rest of the laminate, the voids were manually filled with black pixels. The void percentage was then determined using a threshold function in the image analysis software, imagej. A summary of the measured void contents along with a sample cross-section are given in Fig. 14. The results confirmed that with increasing

pressure at the outlet, the degassing effect was minimized and the overall void content tended to decrease.

#### Flexural

Flexural testing was carried out in accordance with ASTM D790 on an MTS insight load testing machine with a 5 kN load cell. A sample area of  $12.7 \times 80 \text{ mm}^2$ , span of 64 mm and loading rate of 2 mm/min were selected. The results are summarized in Fig. 15.

Two key findings were revealed by the flexural testing. First, among the studied treatments, the untreated fabrics resulted in the best flexural properties (albeit marginally) as verified by ANOVA ( $p < 0.001$ ). On the other hand, the lowest properties were exhibited by the alkaline treatment, likely due to a lower fiber  $V_f$ . The second finding was that with increasing void content the flexural properties of the composites decreased. This is consistent with what has been observed for conventional composites [35]. The samples that experienced the 50 kPa post-fill pressure showed the most pronounced increase in mechanical properties due to lower void content.

#### Charpy Impact

Charpy impact testing was carried out in accordance with ISO 179 in an edgewise parallel configuration. A sample area of  $12.7 \times 80 \text{ mm}^2$  was selected with a span of 60 mm. The frictional loss induced by the setup was measured prior to the tests and taken into account. The results are shown in Fig. 16.

Figure 16 suggests that there was no clear trend between the various treatments and the measured Charpy impact strengths. The same was indicated for the effect of voids on the Charpy impact properties. However, the large coefficient of variance ( $\sim 15\%$ ) indicates that a more suitable impact test configuration may be required for this type of material.

**Fig. 15** Flexural properties of flax/epoxy composites manufactured by resin infusion at different post-fill pressures using common chemical treatments: **a** modulus, **b** modulus versus void content, **c** strength and **d** strength versus void content

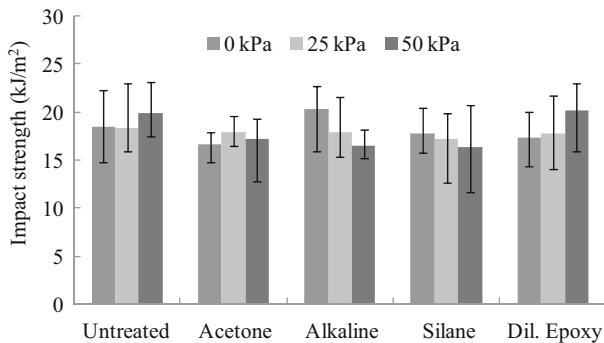
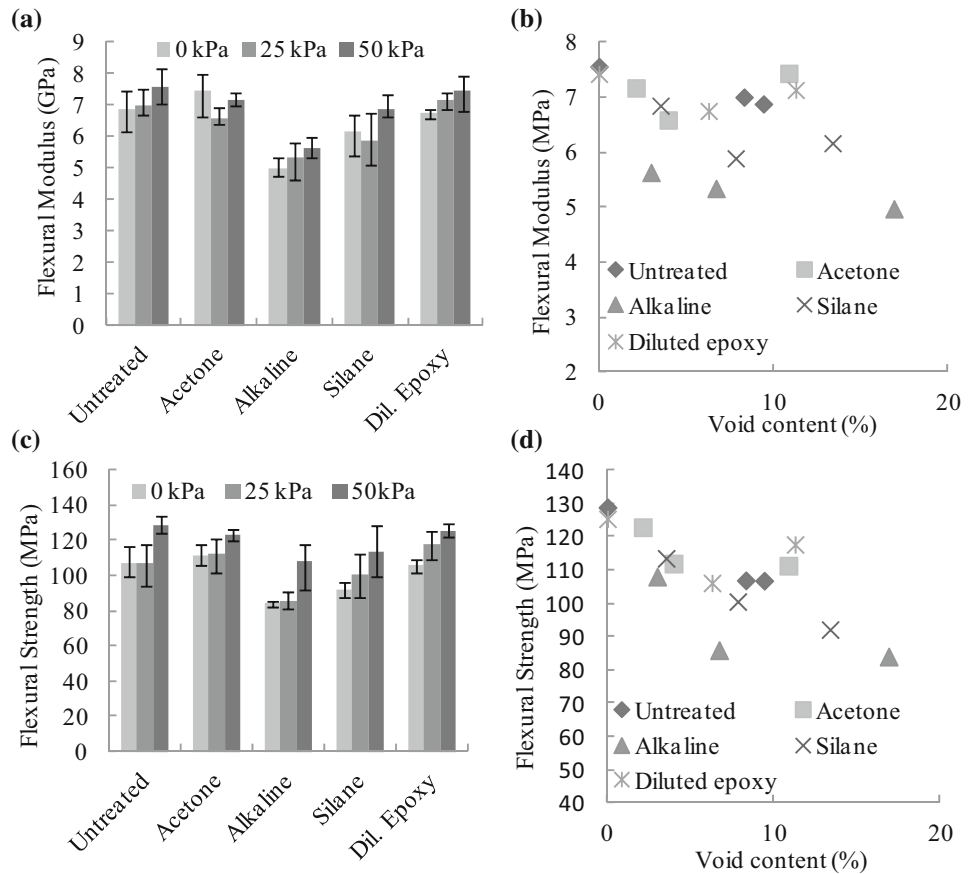


**Fig. 16** Charpy impact properties of flax/epoxy composites manufactured by resin infusion at different post-fill pressures (0, 25 and 50 kPa) using common chemical treatments

## Conclusions

This study dealt with the effects of alkaline, silane and diluted epoxy treatments on the process kinetics of flax fabrics during the resin infusion process and the mechanical properties of the resulting composites. FTIR, SEM and advancing contact angle analysis on the treated fabrics revealed distinct changes in the morphology and chemistry. Laminates were then manufactured by resin infusion on an instrumented tool plate through which the equivalent

permeability and compaction behavior were monitored. The equivalent permeability values and dry compaction responses were shown to not vary significantly. An exception was the alkaline treatment which resulted in a 50 % increase in equivalent permeability likely due to an increase in porosity. This was attributed to fiber swelling and suggests that the fabric boundary condition during treatment is an important parameter in the context of composite processing. A comparison of the flow front evolution data with that predicted by a 1D resin infusion process model confirmed that the observed changes in surface energy would not result in significant changes in infusion time for the given porosity range. Flexural and Charpy impact tests were finally carried out on the manufactured panels. The former test demonstrated the negative impact of voids on flexural strength and modulus. This study suggests that there is not a significant change in processing time during resin infusion for the measured changes in surface energy in the studied porosity range. However, changes in flax fiber morphology such as an increase in fibrillation as a result of chemical treatments can significantly affect the processing kinetics.

**Acknowledgments** The financial support of the Network for Innovative Plastic Materials and Manufacturing Processes (NIPMMP) is

acknowledged. The authors would like to thank Libeco-Lagae® for supplying the fabrics and the Catholic University of Leuven for use of its dynamic tensiometer. The authors would also like to thank Carlos Fuentes Rojas and Le Quan Ngoc Tran for fruitful discussions regarding contact angle measurement. The assistance from Dr. Arthur Levy with the modelling is also kindly acknowledged.

## References

- Bledzki AK, Gassan J (1999) *Prog Polym Sci* 24:221
- Van de Weyenberg I, Ivens J, De Coster A, Kino B, Baetens E, Verpoest I (2003) *Compos Sci Technol* 63:1241
- Rodríguez ES, Stefani PM, Vázquez A (2007) *J Compos Mater* 41:1729
- Umer R, Bickerton S, Fernyhough A (2011) *Compos Part A Appl Sci Manuf* 42:723
- Francucci G, Rodríguez ES, Vázquez A (2010) *Compos Part A Appl Sci Manuf* 41:16
- Masoodi R, Pillai KM (2011) *Handbook of bioplastics and biocomposites engineering applications*. Wiley, Hoboken
- Re C, Bizet L, Breard J (2010) *Proceedings of 10th international conference on flow processes in composite materials (Ascona, Switzerland)*
- Sain M, Rouison D, Couturier M, Panthapulakkal S (2006) *Polym Polym Compos* 14:229
- Bréard J, Henzel Y, Trochu F, Gauvin R (2003) *Polym Compos* 24:391
- Pillai KM, Advani SG (1998) *J Compos Mater* 32:1753
- Lawrence JM, Neacsu V, Advani SG (2009) *Compos Part A Appl Sci Manuf* 40:1053
- Lee GW, Lee NJ, Jang J, Lee KJ, Nam JD (2002) *Compos Sci Technol* 62:9
- Robitaille F, Gauvin R (1998) *Polym Compos* 19:198
- Umer R, Fernyhough A, Bickerton S (2007) *Compos Part A Appl Sci Manuf* 38:434
- Francucci G, Rodríguez ES, Vázquez A (2012) *J Compos Mater* 46:155
- Ouagne P, Bizet L, Baley C, Bréard J (2010) *J Compos Mater* 44:1201
- Baley C, Busnel F, Grohens Y, Sire O (2006) *Compos Part A Appl Sci Manuf* 37:1626
- Volpe CD, Siboni S (1997) *J Colloid Interface Sci* 195:121
- Owens DK, Wendt RC (1969) *J Appl Polym Sci* 13:1741
- Holmberg K, Shah DO, Schwuger MJ (2002) *Handbook of applied surface and colloid chemistry*. Wiley, New York
- Cantero G, Arbelaz A, Llano-Ponte R, Mondragon I (2003) *Compos Sci Technol* 63:1247
- Aziz SH, Ansell MP (2004) *Compos Sci Technol* 64:1219
- Wong K, Yousif B, Low K (2010) *J Mater Des Appl* 224:139
- Karmakar SR (1999) *Chemical technology in the pre-treatment processes of textiles*. Elsevier, Amsterdam
- Chen R, Dong C, Liang Z, Zhang C, Wang B (2004) *Polym Compos* 25:146
- Francucci G, Vázquez A, Ruiz E, Rodríguez ES (2012) *Polym Compos* 33:1593
- Ahn KJ, Seferis JC, Berg JC (1991) *Polym Compos* 12:146
- Comyn J (2006) *Handbook of adhesives and sealants*. Elsevier, Amsterdam
- Amico S, Lekakou C (2001) *Compos Sci Technol* 61:1945
- Baley C (2002) *Compos Part A Appl Sci Manuf* 33:939
- Hammami A, Gebart B (2000) *Polym Compos* 21:28
- Croteau-Labouly B (2007) *Caractérisation combinée de la perméabilité et de la compaction des renforts fibreux dans les procédés de fabrication des composites par infusion*. (École polytechnique de Montréal Thesis, Montreal)
- Terzaghi K (1943) *Theoretical soil mechanics*. Wiley, New York
- Grimsley BW, Hubert P, Song X, Cano RJ, Loos AC, Pipes RB (2001) *Proceedings of 33rd international SAMPE technical conference (Seattle, Washington)*
- Judd NCW, Wright WW (1978) *Sampe J* 14:10